THE ASTROPHYSICAL JOURNAL, 276:524–532, 1984 January 15

THE HIGH-IONIZATION AND EXCITED-STATE INTERSTELLAR LINES IN THE CARINA NEBULA: A GIANT H II REGION IN ABSORPTION

NOLAN R. WALBORN[1,2]
Laboratory for Astronomy and Solar Physics, NASA Goddard Space Flight Center
JOY N. HECKATHORN[2]
Astronomy Department, Computer Sciences Corporation
AND
JAMES E. HESSER[2]
Dominion Astrophysical Observatory, Herzberg Institute of Astrophysics
Received 1983 April 21; accepted 1983 June 28

ABSTRACT

The dominant component of the highly ionized and excited-state interstellar species seen in the ultraviolet toward stars within the Carina Nebula has been found to have a heliocentric radial velocity of about -30 km s^{-1}. This velocity is known to correspond to the near edge of the expanding H II region, as shown by the double optical nebular emission lines and the single He I λ3889 nebular absorption line. It is also seen as a (nondominant) component in both the optical and ultraviolet low-ionization interstellar lines, discussed previously. Hence, the Carina Nebula provides a clear case in which the principal high-ionization interstellar features are associated with the hot stars against which they are observed; and a considerable range of *absorption* lines can provide physical information about the H II region. Also, the weaker zero-velocity, line-of-sight component in the high-ionization species can be measured in this direction relatively free from confusion by the material associated with the stars. There is in addition a pervasive high-ionization feature with a velocity of -90 km s^{-1} in this region, which has the relatively large value of N(C IV)/N(Si IV) = 4.5.

Subject headings: interstellar: abundances — nebulae: H II regions — nebulae: individual — ultraviolet: spectra

I. INTRODUCTION AND OBSERVATIONS

The interstellar absorption line profiles formed within the Carina Nebula (NGC 3372) have been shown to be exceptionally complex, with as many as 12 velocity components in a single line of sight and an overall velocity range of 550 km s^{-1}. The optical Ca II and Na I profiles have been discussed by Walborn (1982), and the low-ionization features at space ultraviolet wavelengths by Walborn and Hesser (1982). In the latter study, based upon observations with the *International Ultraviolet Explorer* (*IUE*) satellite, radial velocities of the various interstellar components were inferred from comparisons of the unique profiles with the accurate optical measurements. However, few if any such relationships were apparent in the case of the high-ionization and excited fine-structure interstellar features also present in the ultraviolet; hence, their discussion was deferred, and it was clear that direct velocity measurements from the *IUE* data would be required. Such measurements have now been performed, and the rather remarkable results will be presented here. The essential result is that the dominant component in the high-ionization and excited-state profiles occurs not near zero velocity, but near -30 km s^{-1} (heliocentric), consistent with the blueshifted near side of the expanding H II region. Furthermore, some of the higher velocity components seen more strongly in the low-ionization interstellar profiles can now be identified in those of high ionization as well. The present results confirm and extend the pertinent conclusions of Laurent, Paul, and Pettini (1982) concerning the interstellar spectrum of HD 93205 in the Carina Nebula.

When the stong interstellar Si IV, C IV, and Al III features were first discovered by *IUE*, considerable discussion arose with regard to their spatial origin. More recently, a consensus has developed to the effect that these lines are most probably formed in the vicinity of the hot stars in whose spectra they are observed (Huber *et al.* 1979; Bruhweiler, Kondo, and McCluskey 1980; Black *et al.* 1980; Cowie, Taylor, and York 1981; Franco and Savage 1982). Because of the fortuitous radial velocity effects, the Carina Nebula provides a particularly clear demonstration of this fact. Furthermore, a considerable array of *absorption* features which may be applied to the physical investigation of ionized nebulae in general now becomes available. Some information regarding column densities, ionization mechanisms, and electron densities is derived here.

The high-resolution *IUE* data upon which the present study is based are those listed by Walborn and Hesser (1982), with the addition of several more recent observations obtained by J. N. H. or from the *IUE* Data Archives and listed in Table 1.

II. MEASUREMENTS

Equivalent widths and velocity displacements of the interstellar line components were measured primarily from Calcomp plots of the appropriate spectral orders, with a scale of 100 km s^{-1} per inch. Most of these plots were made with the Modcomp computer at DAO; however, images newly acquired for this paper were plotted at GSFC

[1] NASA/National Research Council Senior Associate.
[2] Guest Observer, *International Ultraviolet Explorer* satellite.

TABLE 1

ADDITIONAL OBSERVATIONS

Star (HD)	Image Number	Exposure Time (min)	Aperture
92740	SWP 15131	9	Large
92809[a]	SWP 15106	150	Large
93129A	SWP 14007	30	Large
93129A	SWP 15026	30	Large
93131	SWP 15132	6	Large
93403	SWP 9673	70	Small

[a] Lortet, Neimela, and Tarsia 1980; Heckathorn, Bruhweiler, and Gull 1982.

using the IBM 3081. Equivalent widths were measured with a planimeter, and velocity displacements were read from the convenient x-axis scale. The *IUE* Regional Data Analysis Facility at GSFC was used to measure equivalent widths and velocity displacements for the Si II* $\lambda\lambda$1264.7, 1265.0 lines, as well as for the O I** λ1306.0 and Si II* λ1309.3 in a few cases. All velocities have been corrected to heliocentric.

The errors due to observational noise and the equivalent-width measurement procedure were estimated from several well-defined, unblended lines of different strengths measured on more than one image of the same star (additional images were acquired from the *IUE* Data Archives for this purpose). The reproducibility of the measurements so estimated ranges over $\pm 10\%$. The lower limit of reliable measurability is estimated to be 25 mÅ. Additional errors exist in determining the profiles; these errors are more difficult to evaluate. For instance, blending is the major source of error in many of the larger equivalent widths. Continuum placement in *IUE* data can be quite uncertain due to noise and broad absorption features; it is the major source of error for faint lines. Errors due to continuum placement and blending can approach 100% in the worst cases.

The velocity determinations are affected by a combination of image processing uncertainties, errors in the line measurements, and intrinsic errors due to blending. *IUE* observations can be used to obtain accurate wavelength information, and thus velocity displacements, only after correction of the image for reseau motion and spectral format shifts due to secular and temperature changes. The technique for correcting spectral images *a posteriori* is described by Thompson, Turnrose, and Bohlin (1982). (All images used in this study were obtained prior to implementation of the automatic correction procedure.) With this technique, a velocity correction was applied to each image. As a means of checking the accuracy of these individual velocity corrections, an array of neutral interstellar lines in each image was measured for displacements with respect to the laboratory wavelengths. These lines, mainly from C I and Cl I, are well distributed throughout the SWP image and are generally strong and unblended. For an individual star, the corrected velocity of an interstellar line should be constant, so a comparison among different images provides an estimate of the precision of the correction technique. The standard deviation was calculated for each of six stars for which more than one observation exists. The mean of these standard deviations is 2.6 km s^{-1}, which can be compared with the 1 $\sigma = 2.0$ km s^{-1} found by Thompson, Turnrose, and Bohlin from a similar analysis of calibration lamp images. The small difference between these two numbers suggests that pointing of the *IUE* is not a major contributor to wavelength errors for single bright stars. Errors in measurements of individual wavelengths are believed to be ± 3 km s^{-1}, based on repeated measurements in the same image. The combination of these random errors in the velocity correction technique and in the measurements is ± 4 km s^{-1}.

Blending of two or more lines causes the minimum flux points to be displaced. A similar problem exists for weak lines which can be "blended" with noise patterns in *IUE* data. These errors are difficult to quantify. Our data indicate the errors for a given velocity component vary significantly from star to star, and occasionally from species to species in a given star, presumably due to the presence of differing amounts of blending. The total error in velocity is no less than ± 4 km s^{-1}, but probably no greater than ± 10 km s^{-1}, for an individual interstellar component.

The heliocentric radial velocities for the interstellar C I and C I* lines discussed above are listed in Table 2. These velocities are near zero in most cases, implying an origin predominantly along the line of sight to the Carina Nebula and not in the H II region, consistent with expectations from the ionization potential and with the results of Laurent, Paul, and Pettini (1982) for HD 93205.

III. RESULTS

The measured heliocentric radial velocities and equivalent widths of the high-ionization and excited-state interstellar lines are given in Table 3, where the stars have been divided into four groups according to their locations within the η Carinae association. The principal result of this investigation

TABLE 2

HELIOCENTRIC RADIAL VELOCITIES OF INTERSTELLAR NEUTRAL CARBON LINES (km s^{-1})

Species	Line (Å)	93204	93205	93162	303308	−59°2600	−59°2603	93130	93206	93222	93146	93131	93129A	93250	93403	92740
C I	1328.8	9	11	8	8	−9	3	8	7	7	−13	...	−7	−14	6	6
	1560.3	4	2	−5	2	−10	5	9	0	0	−11	3	−7	−1	−2	7
	1656.9	1	3	...	1	−3	−3	6	−2	−3	−9	5	−9	0	6	11
C I*	1329.1	13	17	0	14	−10	−4	16	15	−10	−18	1	−14	−3	4	1
	1560.7	2	1	0	0	−7	10	−5	0	−15	−6	...	−12	−6	...	8
	1656.3	4	6	...	6	−2	8	14	...	...	−5	5	−20	−6	−5	3
	1657.4	3	−1	..	−1	−9	...	−2	3	−8	−17	4	−9	−2	0	6
	1657.9	−1	7	−3	5	−4	3	2	...	−14	−6	3	−9	3	−2	13

NOTE—Stellar identifications: HD/HDE/CPD.

TABLE 3

HELIOCENTRIC RADIAL VELOCITIES AND EQUIVALENT WIDTHS FOR HIGH-IONIZATION AND EXCITED-STATE INTERSTELLAR LINES IN THE CARINA NEBULA

A. Adjacent to η Car

Line (Å)	HD 93204				HD 93205				HD 93162			HDE 303308			
Si IV 1393.8 (km s^{-1})	-87	-31	+ 5		-87	-31	+19		-87	-32			-42		
(mÅ)	56	191	55		33	237	32		152	335			442b		
Si IV 1402.8	-101	-31	+29:		-88	-33	+ 2		-75	-27			-46		
	18	181	33		23	200	28		172	243			369b		
C IV 1548.2	- 88	-38	0		-94	-34	+ 2	+ 56	-80	-30	+155		-46		
	101	221	98		109	217	121	56	227	349	44		445b		
C IV 1550.8	- 98	-40	+ 1		-98	-38	- 3	+ 59	-88	-39	+156		-52		
	65	184	59		53	181	72	17	120	247	23		298		
Al III 1854.7		-32	- 2	+68		-29	+ 8		-68	-18			-33	+73	
		233	145	27		248	102		65	375			461	32	
Al III 1862.8		-35	+ 5	+47		-35	0		-66	-21			---		
		211	84	32		186	68		56	287			---		
O I* 1304.9		-33				-33				-20			---		
		77				91				147			---		
O I** 1306.0		-34			-90	-34				-23			-37	-13	
		148			41	108				196			88	64	
Si II* 1309.3		-35			-96	-35				-24			-36		
		104			24	93				148			81		
Si II* 1264.7	-95	-35:	+96	+134	-86	-35:		+107		-28		-107	-28:	+69	+98
	116	b	29	43	98	b		23		406(b?)		91	b	33	55
Si II* 1265.0		-35:				-39				-28			-42		
		b				113				162			139		

Line (Å)	CPD -59° 2600					CPD -59° 2603						
Si IV 1393.8 (km s^{-1})		-80	-35			-159	- 81	-41	- 6			
(mÅ)		223	256			27	133	208	48			
Si IV 1402.8		-75	-42			-169		-45	-12			
		146	202			15:		147	58			
C IV 1548.2	-151	-76	-36	+12	+94:	-144	-99	-39	- 6	+16	+73	+111
	48	319:	187:	45	43:	95	155	217	65	102	52	49
C IV 1550.8	-159	-83	-50	0:		-132	-102	-42	-17:	+23	+83	+123
	25	193	196	52:		93	111	179	69	84	39	50
Al III 1854.7			-31					-36				
			333:					335				
Al III 1862.8			-33					-36	- 1			
			248					201	52			
O I* 1304.9			---					-32				
			---					90				
O I** 1306.0			-31					-41				
			141					102				
Si II* 1309.3			-34					-37				
			94					114				
Si II* 1264.7	-170	-83	-35		+114	-220		-33				
	33	69(b?)	152(b?)		24	56		202				
Si II* 1265.0			-35					-42				
			103					94				

TABLE 3—*Continued*

B. South of η Car

Line (Å)	HD 93130			HD 93206			HD 93222					HD 93146			HD 93131		
Si IV 1393.8 (km s^{-1})		-52	- 8	-74	-14	+11			-36			-83	-21	+59:		-38	
(mÅ)		319	182	175	224	208			340			218	418	39:		546:b	
Si IV 1402.8		-51	-12	-84	-24:	+ 4		-77	-37	+ 5		-90:	-28	+49		-35	
		315	142	95	181:	185		104	231	140		200:b	360	62		252b	
C IV 1548.2		-40	- 1	-80	+ 3		-350	-64	-24	+13	+62	-86	-31	+40	-81	-45	+ 4:
		350	188	244	357b		71	252	190	68	25	255	323	50	187	260	82:
C IV 1550.8		-52	- 7	-82	-17		-349	-78	-28	+11	+70	-83	-33	+42	-82	-45	+15:
		260	141	171	264b		43	195	132	53	35	231	232	33	126	219	30:
Al III 1854.7		-21		-80	0	+105			-20	+ 7:			-32			-37	
		484		93	534b	29			289	182			567			425	
Al III 1862.8		-22		-88	- 3	+110			-19	+19:		-98:	-35			-25	
		374		56	479b	28			232	64		38:	355			287	
O I* 1304.9		-18			---				---				-22			---	
		42			---				---				73			---	
O I** 1306.0		-21			---				-24				-16			---	
		61			---				57				132			---	
Si II* 1309.3		-22			-27	- 1			-24				-33			-26	
		107			69	52			86				136			55	
Si II* 1264.7	-186	-20			---			-85	-25			-98	-39			-32	
	57	216			---			60	241(b?)			68	284			160	
Si II* 1265.0	-175	-22			---				-34				-42			-43	
	53	112			---				103				128			55	

C. North of η Car and Periphery

Line (Å)	HD 93129A			HD 93250						HD 93403		HD 92740			HD 92809	
Si IV 1393.8 (km s^{-1})	-101	-39	+50			-35	+20			-47:	+ 8:	-62	- 2	+18		---
(mÅ)	153	376	56			361	97			40	388	32	85	45		---
Si IV 1402.8	-102	-39	+46			-31	+14		+101	-51:	- 1	-84:	-24	+ 6	-54	-29
	50	347	39			342	85		30	30	243	9:	68	27	173	184
C IV 1548.2	-103	-41	+59			-29	+ 7	+67	+ 92	-25	+15	-57		0		-37
	196	429	16			373	92	58	74	161	177	100		115		430b
C IV 1550.8	-108	-37	+66			-32	+ 8	+68	+ 88	-24	+26	-62		+12		-38
	120	407	23			293	88	23	48	187	71	38		69		306b
Al III 1854.7	-109	-36		- 93	-48	-18					+22		-13			-17
	93:	471		42	160	245					299		231			571b
Al III 1862.8	-119	-39		-103	-60	-20					+17		-16			-35
	30	337		54	110	216					181		145			406b
O I* 1304.9		-21				-20	+ 4				---			+ 7		- 7:
		54				108	96				---			43		53
O I** 1306.0		-22:				-15	+ 7				+23:			+ 2:		+ 5:
		77				173	101				49:			40		81
Si II* 1309.3		-36				-17					+13		-17			-17
		108				131					59		76			62
Si II* 1264.7		-38				---					- 6		-13			-28
		246				---					136		118			212
Si II* 1265.0		-47	+40			---					---		-22			-25
		154	40			---					---		39			37

b: blended feature measured as a whole.

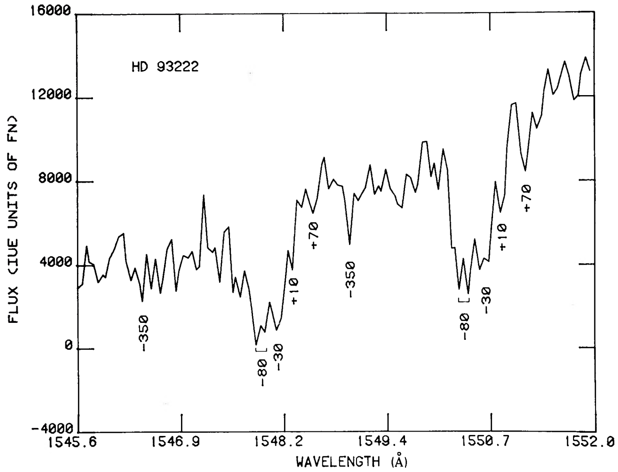

FIG. 1

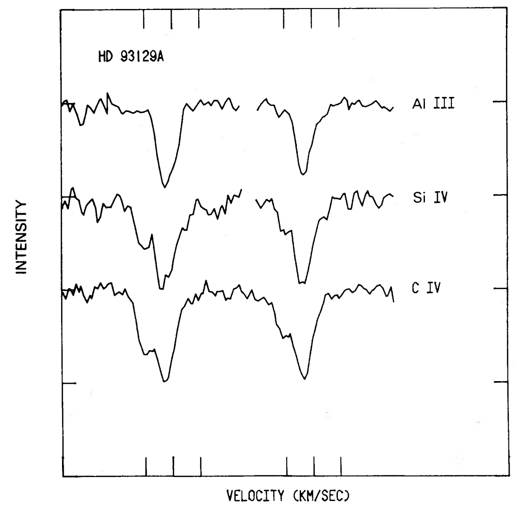

FIG. 2

FIG. 1.—Profiles of interstellar C IV $\lambda\lambda$1548.2, 1550.8 in the spectrum of HD 93222, with the measured velocity components indicated (km s^{-1}). FN = flux number.

FIG. 2.—Normalized profiles of the high-ionization interstellar lines in the spectrum of HD 93129A. The horizontal marks indicate the zero and/or the continuum levels for successive profiles, while the vertical marks denote 0 and $\pm$100 km s^{-1} heliocentric for each profile.

can be appreciated by inspection of the table: *in nearly every profile the strongest component has a substantially negative velocity, with an overall average near -30 km s^{-1}* (excluding the peripheral stars HD 92740, 92809, and 93403). In a few cases a higher negative velocity component is somewhat stronger (HD 93222, CPD $-59°2600$), or blending with the zero-velocity component obscures the issue (HD 93206), but the general result is quite definite. A second noteworthy result is the ubiquity throughout the region of a high-ionization feature with a velocity near -90 km s^{-1}; in fact, it is present in all the spectra except those of the three peripheral stars and of HD 93130 and HDE 303308, although the excessively negative velocity of the "-30 km s^{-1}" component in these last two cases may be due to blending with a more negative one.

In general, the very high velocity features are most prominent in Si II* λ1264.7; in this respect it behaves similarly to C II* λ1335.7, discussed by Walborn and Hesser (1982). Of the high-ionization lines, the C IV doublet appears to be most sensitive to the very high velocity features; the profiles toward HD 93222 (Fig. 1) and CPD $-59°2603$ are perhaps the most spectacular, although reobservations with greater signal-to-noise ratios are desirable to definitively confirm all of the components measured here.

While the recognition of the -30 km s^{-1} and -90 km s^{-1} features permits substantial organization of the present phenomena as well as elucidation of their relationships to the low-ionization features discussed previously, nevertheless, the high-ionization results also serve to increase the overall complexity of the interstellar characteristics observed in this region. This result follows from comparisons both between the high- and low-ionization features, and among the various high-ionization features themselves. As an example of the former, the optical -90 km s^{-1} interstellar feature is prominent only in a relatively compact group of stars adjacent to η Car (Walborn 1982), whereas the high-ionization feature at that velocity apparently pervades the entire nebula; this circumstance raises a basic question about the physical identity of these features. Another specific example is provided by HD 93129A, which has no high-velocity interstellar components in the optical but does have well developed components at about -100 km s^{-1} and $+50$ km s^{-1} in the high-ionization lines (Fig. 2). As instances of the variety among the high-ionization features themselves, one may consider the strikingly different Si IV profiles between the adjacent stars CPD $-59°2600$ and $-59°2603$ (Fig. 3). Also remarkable is the frequently systematic difference between the behavior of Si IV and C IV on the one hand, and Al III on the other. Perhaps the most extreme example of this effect is provided by HD 93250 (Fig. 4), in which Si IV and C IV show only high positive velocity components, while Al III shows only high negative ones! Similar contrasts among the various high-ionization profiles can be seen in the spectra of HD 93204 (Fig. 5) and HD 93206 (Fig. 6).

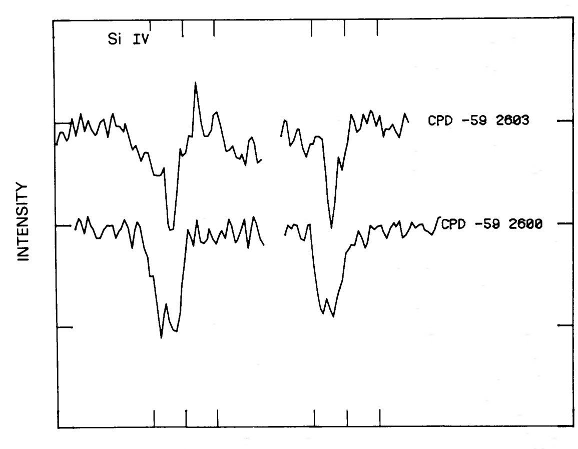

FIG. 3.—Normalized profiles of interstellar Si IV $\lambda\lambda$1393.8, 1402.8 in the spectra of CPD $-59°2600$ and $-59°2603$. Scales as in Fig. 2. Note the striking difference in the relative prominence of the feature near -80 km s^{-1} between these two adjacent stars.

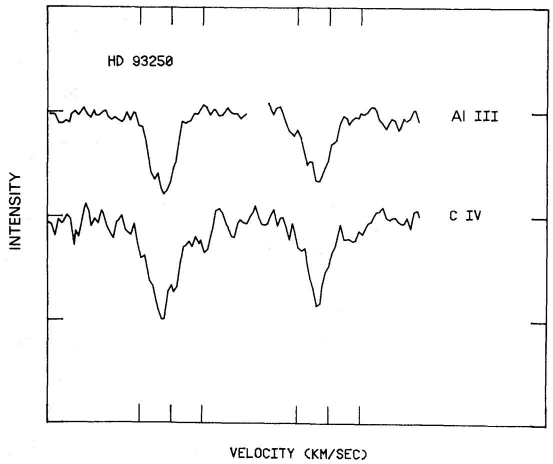

FIG. 4

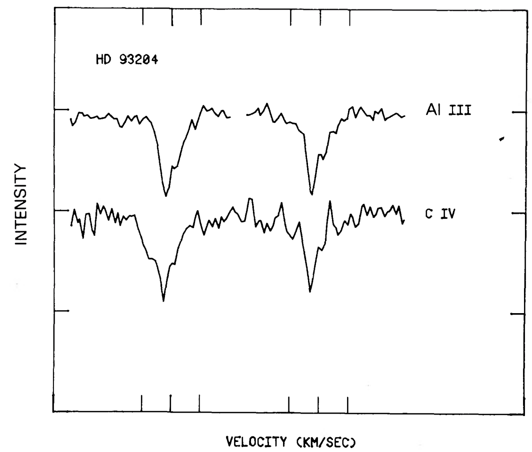

FIG. 5

FIG. 4.—Normalized profiles of interstellar C IV and Al III in the spectrum of HD 93250. Scales as in Fig. 2. Note the presence of high positive velocity components in C IV, but of high negative velocity ones in Al III.

FIG. 5.—Same as Fig. 4 for HD 93204.

Finally, an example of the rich $\lambda1300$ region, which contains three of the excited fine-structure lines, is illustrated in Figure 7 (HD 93205). Here it should be noted that Si II $\lambda1304.4$ and O I* $\lambda1304.9$ are separated by 112 km s^{-1}, so that simultaneous components near, e.g., +80 km s^{-1} in the former and -30 km s^{-1} in the latter will be completely overlapped. Such a situation does in fact occur in the spectra of HD 93222, HDE 303308, and CPD $-59°2600$; the corresponding equivalent widths given for the Si II line in Tables 3 and 4 of Walborn and Hesser (1982) therefore include the O I* contribution.[3]

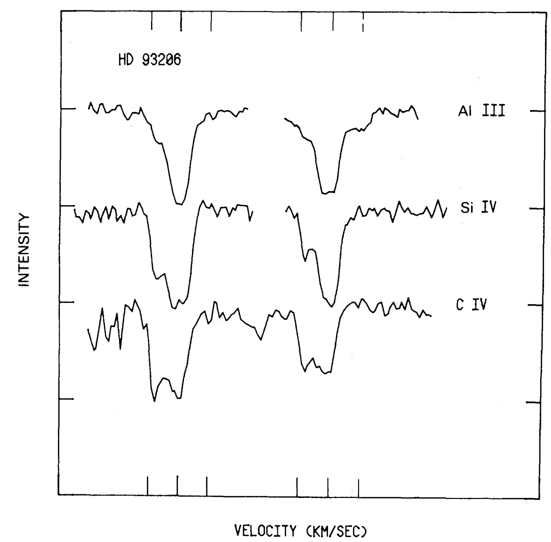

FIG. 6.—Same as Fig. 2 for HD 93206.

IV. ANALYSIS

a) *Curves of Growth, Velocity Dispersions, and Column Densities*

The -30 km s^{-1} and -90 km s^{-1} features have been analyzed by means of the Spitzer (1978) curve of growth. An individual species in a given spectrum provides minimal information regarding the appropriate curve; hence, the velocity dispersion indicated by each species in each spectrum was determined separately, and an average was found for the feature in question. Initially the northern and southern regions of the nebula were considered separately, but the resulting velocity dispersions were the same for the corresponding features in each region, so all spectra showing the features of interest have been combined for the curve-of-growth analysis. The derived velocity dispersions are 20 ± 1 km s^{-1} (standard deviation of the mean, $n = 37$) for the -30 km s^{-1} feature, and 15 ± 2 km s^{-1} ($n = 14$) for the -90 km s^{-1}; the

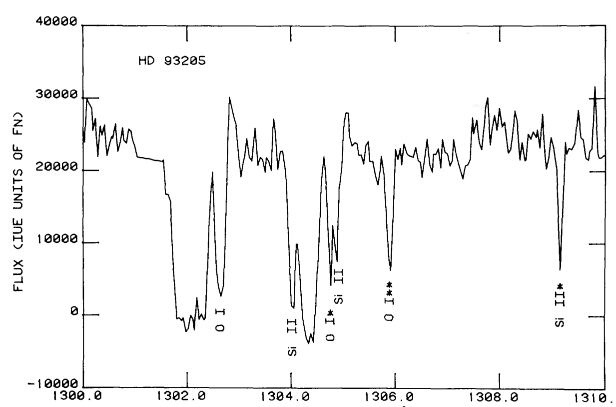

FIG. 7.—Interstellar lines in the $\lambda1300$ region of HD 93205. The discrete velocity components identified are O I $\lambda1302.2$ at +100 km s^{-1}; Si II $\lambda1304.4$ at -90 and +100 km s^{-1}; O I* $\lambda1304.9$ at -30 km s^{-1}; O I** $\lambda1306.0$ at -30 km s^{-1}; and Si II* $\lambda1309.3$ at -30 km s^{-1}. A reseau mark has been omitted just below the O I profile.

[3] The high positive velocity components in CPD $-59°2600$ require further component. The optical Ca II profile shows a stronger component at +90 km s^{-1} and a weaker blend of components at +126 and +132 km s^{-1} (Walborn 1982). Walborn and Hesser (1982) interpreted the dominant feature in the low-ionization ultraviolet lines as occurring at +120 km s^{-1}. However, the present velocity measurements reveal a more complex situation (the additional image SWP 7987 was also measured), as follows: O I $\lambda1302$, +96 km s^{-1}; Si II $\lambda1304$, +96 km s^{-1}; C II* $\lambda1335$, +98 km s^{-1}; Si II $\lambda1526$, +108 km s^{-1}; Fe II $\lambda1608$, +115 km s^{-1}; Al II $\lambda1670$, +113 km s^{-1}; Fe II $\lambda2599$, +100 km s^{-1}; Mg II $\lambda2795$, +102 km s^{-1}; Mg II $\lambda2802$, +112 km s^{-1}; and Mg I $\lambda2852$, +108 km s^{-1}. These results indicate that different components dominate in different lines, and higher resolution will be necessary for a definitive interpretation.

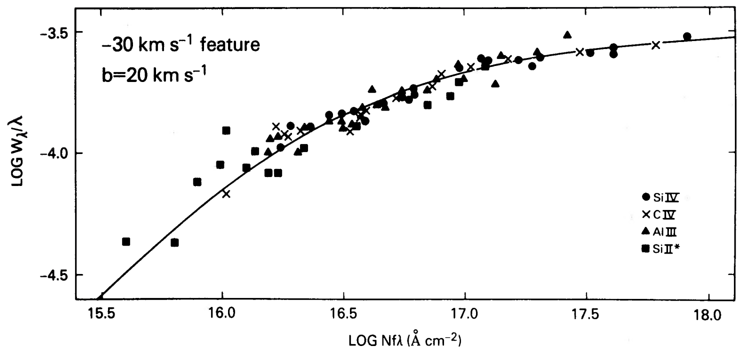

FIG. 8.—Curve of growth for the -30 km s^{-1} feature. All suitable components at or near that velocity have been fitted to the theoretical curve, which was chosen as described in the text.

two curves of growth are shown in Figures 8 and 9, respectively, and the column densities are given in Table 4. The column densities from the single O I* and O I** transitions have, of course, been read from the curves defined by the other species, as have the column densities in other cases when only a single transition (or in the case of Si II*, only the similarly intense λλ1265.0 and 1309.3) was measurable.

The C IV and Si IV column densities for the -90 km s^{-1} feature toward HD 93204 and 93205 would have a negligible effect on the abundances and depletions found from C II and Si II by Walborn and Hesser (1982), substantiating the previous assumption that the singly ionized states are the dominant ones. However, as discussed elsewhere, the physical identity of the high- and low-ionization features at -90 km s^{-1} is not obvious, because of their different spatial distributions.

b) *N*(C IV)/*N*(Si IV) *Ratios*

The ratios of the C IV and Si IV column densities potentially provide information about the ionization mechanisms involved (Franco and Savage 1982, and references therein). The results found here for the -30 km s^{-1} and -90 km s^{-1} features toward the Carina Nebula are given in Table 5. The relatively small value for the -30 km s^{-1} feature is consistent with UV photoionization, while the significantly larger result for the -90 km s^{-1} feature is indicative of a contribution by collisional or X-ray ionization.

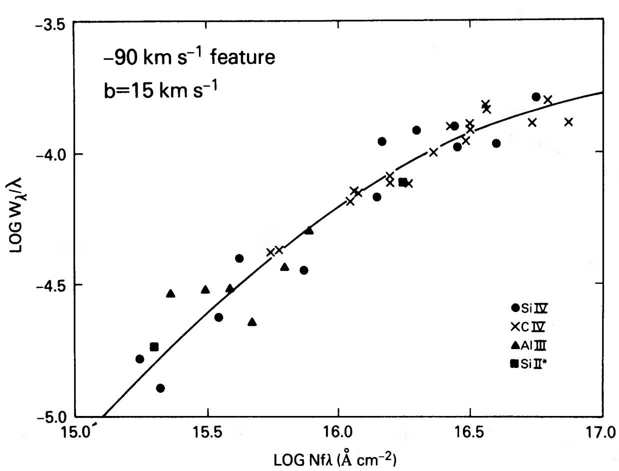

FIG. 9.—Same as Fig. 8 for the -90 km s^{-1} feature.

c) *Electron Densities*

The relative intensities of the excited fine-structure transitions carry information about the temperature and electron density of the interstellar absorbing material. Application of the method here is hampered by the generally complete blending of the strong zero-volt lines in the case of the -30 km s^{-1} feature (Walborn and Hesser 1982), and by undetectability of the weaker excited-state lines from the -90 km s^{-1} feature. However, intensity estimates for the -30 km s^{-1} component in Si II λ1304.4 toward HD 93204 and 93205 have been obtained here for this purpose; they are 173 and 274 mÅ, respectively. This component is better resolved in HD 93204, and hence the measurement is more reliable, than in HD 93205, shown in Figure 7. The corresponding column densities have been read from Figure 8. Also, for the -90 km s^{-1} feature toward these two stars, both Si II* (Table 4) and Si II (Walborn and Hesser 1982) column densities are available. The electron densities for these four cases, as implied by the formulation of Smeding and Pottasch (1979), are given in Table 6. A temperature of 10^4 K has been assumed for the -30 km s^{-1} feature, consistent with its identification as the expanding H II region. The more reliable result from the spectrum of HD 93204 is in perfect agreement with the average electron densities derived from [O II] and [S II] emission lines for two regions (1a and 1b) near these stars by Peimbert, Torres-Peimbert, and Rayo (1978).

V. DISCUSSION

a) *The* -30 km s^{-1} *Feature*

The nebular emission lines from the Carina Nebula are typically double with a separation between the components of around 35 km s^{-1} (Walborn and Hesser 1975; Deharveng and Maucherat 1975). The nebular absorption line He I λ3889, on the other hand, is always single with a heliocentric radial velocity near -30 km s^{-1}, in agreement with the shortward component of the double emission lines; this circumstance strongly indicates that the H II region is expanding, and that the negative-velocity material is in front of the stars while the positive-velocity material lies beyond them (Walborn and Hesser 1975). The ubiquitous components in the optical Ca II and Na I interstellar absorption lines with velocities between -20 and -40 km s^{-1} have likewise been identified with the overall expansion of the Carina Nebula (Walborn 1982). With this background, the dominant -30 km s^{-1} feature

TABLE 4

LOG COLUMN DENSITIES (cm^{-2})

	HD 93204		HD 93205		HD 93162		HDE 303308	
Species	-90 km s^{-1}	-30 km s^{-1}	-90 km s^{-1}	-30 km s^{-1}	-90 km s^{-1}	-30 km s^{-1}	-90 km s^{-1}	-30 km s^{-1}
Si IV	12.76	13.72	12.68	13.88	13.74	14.23	--	--
C IV	13.56	14.09	13.59	14.09	14.08	14.49	--	14.67[a]
Al III	--	13.50	--	13.50	12.80	13.89	--	14.35[a]
O I*	--	14.10[a]	--	14.20[a]	--	14.51[a]	--	--
O I**	--	14.51[a]	13.82[a]	14.30[a]	--	14.74[a]	--	14.18[a]
Si II*	13.23[a]	13.79[a]	13.21	13.93[a]	--	14.20[a]	13.05[a]	14.01[a]

	CPD −59° 2600		CPD −59° 2603		HD 93130	HD 93206		HD 93222	
	-90 km s^{-1}	-30 km s^{-1}	-90 km s^{-1}	-30 km s^{-1}	-30 km s^{-1}	-90 km s^{-1}	-30 km s^{-1}	-90 km s^{-1}	-30 km s^{-1}
Si IV	13.89	13.93	13.43[a]	13.68	14.41	13.58	13.80	13.54[a]	14.21
C IV	14.37[a]	14.06:	13.88	14.09	14.53	14.31	--	14.25	13.84
Al III	--	13.75	--	13.61	14.30	12.89	--	--	13.64
O I*	--	--	--	14.18[a]	13.79[a]	--	--	--	--
O I**	--	14.47[a]	--	14.26[a]	13.99[a]	--	--	--	13.95[a]
Si II*	12.88:[a]	13.77[a]	--	13.81	13.91	--	13.57[a]	12.80[a]	13.85[a]

	HD 93146		HD 93131		HD 93129A		HD 93250	
	-90 km s^{-1}	-30 km s^{-1}	-90 km s^{-1}	-30 km s^{-1}	-90 km s^{-1}	-30 km s^{-1}	-90 km s^{-1}	-30 km s^{-1}
Si IV	14.03[a]	15.05	--	--	13.30	14.75	--	14.65
C IV	14.38	14.42	14.02	14.26	14.02	15.30	--	14.69
Al III	--	14.44	--	13.98	12.60[a]	14.15	12.67	13.53
O I*	--	14.08[a]	--	--	--	13.92[a]	--	14.30[a]
O I**	--	14.42[a]	--	--	--	14.01[a]	--	14.63[a]
Si II*	12.87[a]	14.05	--	13.52	--	13.93	--	13.94[a]

[a] Value read from the curves of growth determined by the other measurements.

of the ultraviolet high-ionization and excited-state interstellar lines in this region is readily interpreted in terms of the expanding ionized nebular material. The inference from the radial velocities is supported by the low N(C IV)/N(Si IV) ratio found above, indicative of UV photoionization in the -30 km s^{-1} feature. The same conclusion has been reached in the individual case of HD 93205 in the Carina Nebula by Laurent, Paul, and Pettini (1982), and analogously from

TABLE 5

C IV/Si IV COLUMN DENSITY RATIOS

STAR (HD/CPD)	FEATURE	
	-30 km s^{-1}	-90 km s^{-1}
93204	2.3	6.3
93205	1.6	8.1
93162	1.8	2.2
−59°2600	1.4	3.0
−59°2603	2.6	2.8
93130	1.3	...
93206	...	5.4
93222	0.43	5.1
93146	0.23	2.2
93129A	3.6	5.2
93250	1.1	...
Mean	1.6	4.5
Standard deviation of mean	±0.3	±0.7

IUE observations of the Orion Nebula exciting stars by Franco and Savage (1982).

The first nebular absorption line to be discovered was He I λ3889 in the Orion Nebula by Wilson (1937); see also Wilson *et al.* (1959). It was subsequently observed in the 30 Doradus (Feast 1953, 1961; Walborn 1980) and Carina (Walborn and Hesser 1975) Nebulae, while Thackeray (1969) discovered He I λ10830 nebular absorption in the latter. It is clear that the high-ionization and excited-state interstellar absorption lines observed toward stars in H II regions arise in the same nebular material producing the He I absorption as well as the emission lines. Hence, an extensive array of absorption lines is now available which can provide information about physical conditions in H II regions complementary to that derived from the emission lines. A similar observation in ultraviolet spectra of planetary nebulae has been made by S. Heap (unpublished).

As also pointed out by Laurent, Paul, and Pettini (1982), the substantial velocity shift of the nebular absorption lines toward the Carina Nebula stars entails the collateral benefit of permitting relatively clean measurements of the weaker high-ionization features near zero velocity, formed along the line of sight through the galactic disk.

b) *The* -90 km s^{-1} *Feature*

The interpretation of this pervasive high-velocity feature in the high-ionization interstellar profiles throughout the Carina

TABLE 6
ELECTRON DENSITIES

Feature (km s^{-1})	Star (HD)	Log N(Si II) (cm^{-2})	Log N(Si II*) (cm^{-2})	Log n_e(10^4 K) (cm^{-3})	Log n_e(10^3K) (cm^{-3})
−30	93204	14.14	13.79	2.5	...
	93205	14.68	13.93	2.0	...
−90	93204	13.92	13.23	2.1	1.8
	93205	14.31	13.21	1.7	1.4

Nebula seems rather less obvious. The basic questions are whether it corresponds physically to the -90 km s^{-1} material seen only adjacent to η Car in the optical and ultraviolet low-ionization profiles, and hence whether it is the same feature in both the northern and southern parts of the Nebula. One possibility is a relationship to the more extensive Carina "supershell" proposed by Cowie *et al.* (1981); however, the absence of the feature in the spectra of the peripheral stars HD 92740, 92809, and 93403 is a difficulty with that identification. It should also be noted that the X-ray observations available so far (Seward *et al.* 1979; Seward and Chlebowski 1982) refer essentially only to the region of the Carina Nebula itself. The relatively large N(C IV)/N(Si IV) ratio in the -90 km s^{-1} feature suggests a contribution from collisional and/or X-ray ionization.

We are grateful to Dr. R. C. Bohlin for advice concerning velocity corrections to *IUE* images, and for generously providing the software necessary to make the Calcomp plots at GSFC. J. N. H. was supported by NASA contract NAS 5-25774.

REFERENCES

Black, J. H., Dupree, A. K., Hartmann, L. W., and Raymond, J. C. 1980, *Ap. J.*, **239**, 502.
Bruhweiler, F. C., Kondo, Y., and McCluskey, G. E. 1980, *Ap. J.*, **237**, 19.
Cowie, L. L., Hu, E. M., Taylor, W., and York, D. G. 1981, *Ap. J.* (*Letters*), **250**, L25.
Cowie, L. L., Taylor, W., and York, D. G. 1981, *Ap. J.*, **248**, 528.
Deharveng, L., and Maucherat, M. 1975, *Astr. Ap.*, **41**, 27.
Feast, M. W. 1953, *Observatory*, **73**, 255.
———. 1961, *M.N.R.A.S.*, **122**, 1.
Franco, J., and Savage, B. D. 1982, *Ap. J.*, **255**, 541.
Heckathorn, J. N., Bruhweiler, F. C., and Gull, T. R. 1982, *Ap. J.*, **252**, 230.
Huber, M. C. E., Nussbaumer, H., Smith, L. J., Willis, A. J., and Wilson, R. 1979, *Nature*, **278**, 697.
Laurent, C., Paul, J. A., and Pettini, M. 1982, *Ap. J.*, **260**, 163.
Lortet, M. C., Niemela, V. S., and Tarsia, R. 1980, *Astr. Ap.*, **90**, 210.
Peimbert, M., Torres-Peimbert, S., and Rayo, J. F. 1978, *Ap. J.*, **220**, 516.
Seward, F. D., and Chlebowski, T. 1982, *Ap. J.*, **256**, 530.
Seward, F. D., Forman, W. R., Giacconi, R., Griffiths, R. E., Harnden, F. R., Jr., Jones, C., and Pye, J. P. 1979, *Ap. J.* (*Letters*), **234**, L55.
Smeding, A. G., and Pottasch, S. R. 1979, *Astr. Ap. Suppl.*, **35**, 257.
Spitzer, L. 1978, *Physical Processes in the Interstellar Medium* (New York: J. Wiley and Sons).
Thackeray, A. D. 1969, *Mem. Roy. Soc. Liege*, **17**, 323.
Thompson, R. W., Turnrose, B. E., and Bohlin, R. C. 1982, *Astr. Ap.*, **107**, 11.
Walborn, N. R. 1980, *Ap. J.* (*Letters*), **235**, L101.
———. 1982, *Ap. J. Suppl.*, **48**, 145.
Walborn, N. R., and Hesser, J. E. 1975, *Ap. J.*, **199**, 535.
———. 1982, *Ap. J.*, **252**, 156.
Wilson, O. C. 1937, *Pub. A.S.P.*, **49**, 338.
Wilson, O. C., Münch, G., Flather, E. M., and Coffeen, M. F. 1959, *Ap. J. Suppl.*, **4**, 199.

JOY N. HECKATHORN: Code 685.9, Goddard Space Flight Center, Greenbelt, MD 20771

JAMES E. HESSER: Dominion Astrophysical Observatory, 5071 West Saanich Road, Victoria, B.C. V8X 4M6, Canada

NOLAN R. WALBORN: Code 683, Goddard Space Flight Center, Greenbelt, MD 20771